Short Communication

Structure and Electrochemical Properties of Hierarchically Porous Silicon Film Prepared with the Combination of Magnetron Sputtering Deposition and Metal-Assisted Chemical Etching

Yan Zhao[1,2], Zhengjun Liu[1], Chunyong Liang[1,2,], M. Yu. Maximov[4], Baoxi Liu[1,2], Junming Wang[3], Fuxing Yin[1,2]*

[1] School of Material Science & Engineering, Research Institute for Energy Equipment Materials, Hebei University of Technology, Tianjin 300130, China
[2] Tianjin Key Laboratory of Materials Laminating Fabrication and Interface Control Technology, Hebei University of Technology, Tianjin 300130, China
[3] Synergy Innovation Institute of GDUT, Heyuan, Guangdong Province, China
[4] Peter the Great Saint-Petersburg Polytechnic University, Saint-Petersburg, 195221, Russia
[*]E-mail: liangcy_hebut@outlook.com

A novel hierarchically porous silicon film on Cu foil was fabricated by employing the combination of magnetron sputtering deposition and metal-assisted chemical etching technology. The as-prepared porous Si film were directly used as working electrodes without adding of binder or electron conductive agent, which exhibited high specific capacities and stable cyclability. Specifically, a high initial discharge capacity of 1976 mAh g^{-1} is attained at a current density of 300 mA g^{-1} and a stable discharge capacity of 1629 mAh g^{-1} obtained after 100 cycles. This superior electrochemical properties could be ascribed to the unique hierarchically porous structure, effectively buffering volume changes during the charge/discharge process.

1. INTRODUCTION

The development of efficient and cheap lithium-ion batteries (LIBs) is highly desirable to meet the requirement of the next-generation electric vehicles [1-3]. Until now, transition metal oxides and silicon, which can reversibly react with lithium, have attracted much attention as the potential candidates for the next generation LIB anode materials, due to high theoretical capacities, low cost and

high safety [4-12]. Among them, silicon has been intensively studied for its high theoretical capacities of 4200 mAh g^{-1} (corresponding to the Li$_{22}$Si$_5$ alloy at room temperature) with a low potential window [4]. In addition, Si also has advantages of natural abundance, low cost and environmental friendliness. Nevertheless, several problems are a big hurdle in the real application of Si anode for LIBs. Si anode suffers the significant volume change (400%) during the lithiation/delithiation process, resulting in the dramatic destruction of the electrode structure and subsequent electrical disconnection from the current collector [10].

So far, progress in the study of Si anodes has been largely benefit by developing nanostructured silicon materials, such as such as Si nanowires, core-shell Si nanowires, hollow Si nanostructure and Si nanoparticles [13-16]. Among the various Si nanostructure, film-like Si nanostructures can provide additional advantages, realizing good adhesion for deposit, ion pass and conductivity, and waive the use of binder materials [17].

In this work, we combined the magnetron sputtering deposition and metal-assisted chemical etching to prepare the porous silicon film. Recently, metal-assisted chemical etching has been introduced to prepared porous silicon due to several advantages besides simple fabricated, low-cost, mild conditions and wafer-scale production. This method has been widely used for solar cells, gas sensor and thermoelectric. Herein, we report a room-temperature etching in aqueous HF solution using metal-assisted chemical etching technology to magnetron-sputtering deposited silicon film, and its physical and electrochemical properties as an anode for LIBs were investigated.

2. EXPERIMENT

Nanoscale and mesoscale films of silicon were deposited on copper foil substrate from a commercial 5-inch diameter Si target (99.999%) at 200 W using radio frequency magnetron sputtering (PerkinElmer-8L). The base pressure in the sputtering chamber was 6×10^{-5} Pa and was maintained a working pressure of 0.6 Pa. Surface oxides from the target were removed after the pre-sputtering was carried out for 20 min at 400 W prior to each deposition. The thickness and weight of the films were determined by a profilometer (Tencor) and an electronic balance (Sartorius CPA225D Semi Micro, Germany), respectively.

The metal-assisted chemical etching method was then applied to silicon film on copper substrate to render it porous silicon nanostructure. In detail, the etching process was performed in a sealed reactor by immersing the substrate into a mix solution of 0.02 M AgNO$_3$ and 1.5 M HF. The reactor was placed in an oven with a constant temperature at 60 ^{o}C. After 300s, the copper foil with porous silicon structure was produced. A diluted nitric acid (10%) was used for removing residual silver particles of the silicon surface. The as prepared sample was finally rinsed with deionized water for several times and dried for 2 h in a vacuum oven at 80 ^{o}C. Besides, all substrates were cleaned with acetone and alcohol followed by drying with compressed nitrogen before deposition and etching processes. The specific surface area and the average pore sizes were examined by the Brunaner-Emmet-Teller (BET) and Barret-Joyner-Halenda (BJH) methods at 77 K (Autosorb iQ, Quantachrome

Corportion). The morphology of the samples were characterized by field-emission scanning electron microscopy (FE-SEM, S4800, Hitachi Limited).

2032 coin-type half-cells were then assembled in an argon-filled glove box. 1 cm^2 punched disks of the porous Si film was used as the working electrode and pure lithium foil as the anode, with a microporous polypropylene film as the separator. The liquid electrolyte was composed of 1 M LiPF$_6$ in 1:1 (v/v) ethylene carbonate/diethyl carbonate (EC/DEC) solvent. The electrochemical characteristics of the batteries were measured by a battery test system (Neware, BTS-5V5 mA) at room temperature. Galvanostatic discharge/charge cycling was carried out in the potential range of 0.01-2.5 V (versus Li$^+$/Li).
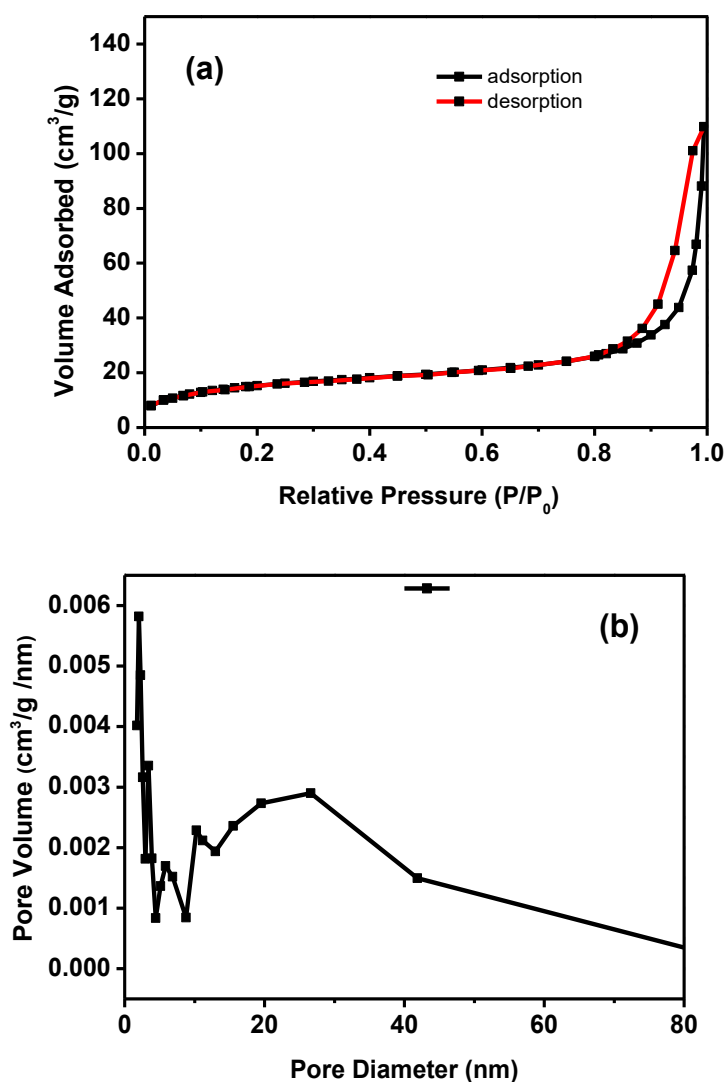
3. RESULTS AND DISCUSSION

Figure 1. a Nitrogen sorption isotherms of porous Si; **1b** Pore size distributions of porous Si.

The pore structures of the prepared porous Si film were analyzed by N_2 adsorption/desorption. As shown in Fig. 1a, the N_2 adsorption isotherms of Si exhibits typical IV isotherm with a H1 hysteresis loop, implying hybrid microporous and mesoporous structure of the samples. And the BET surface area of porous Si is 87.850 m^2 g^{-1}. Meanwhile, the BJH pore size distributions of porous Si are given in Fig. 1b, which reaches to 0.667 cm^3 g^{-1}.
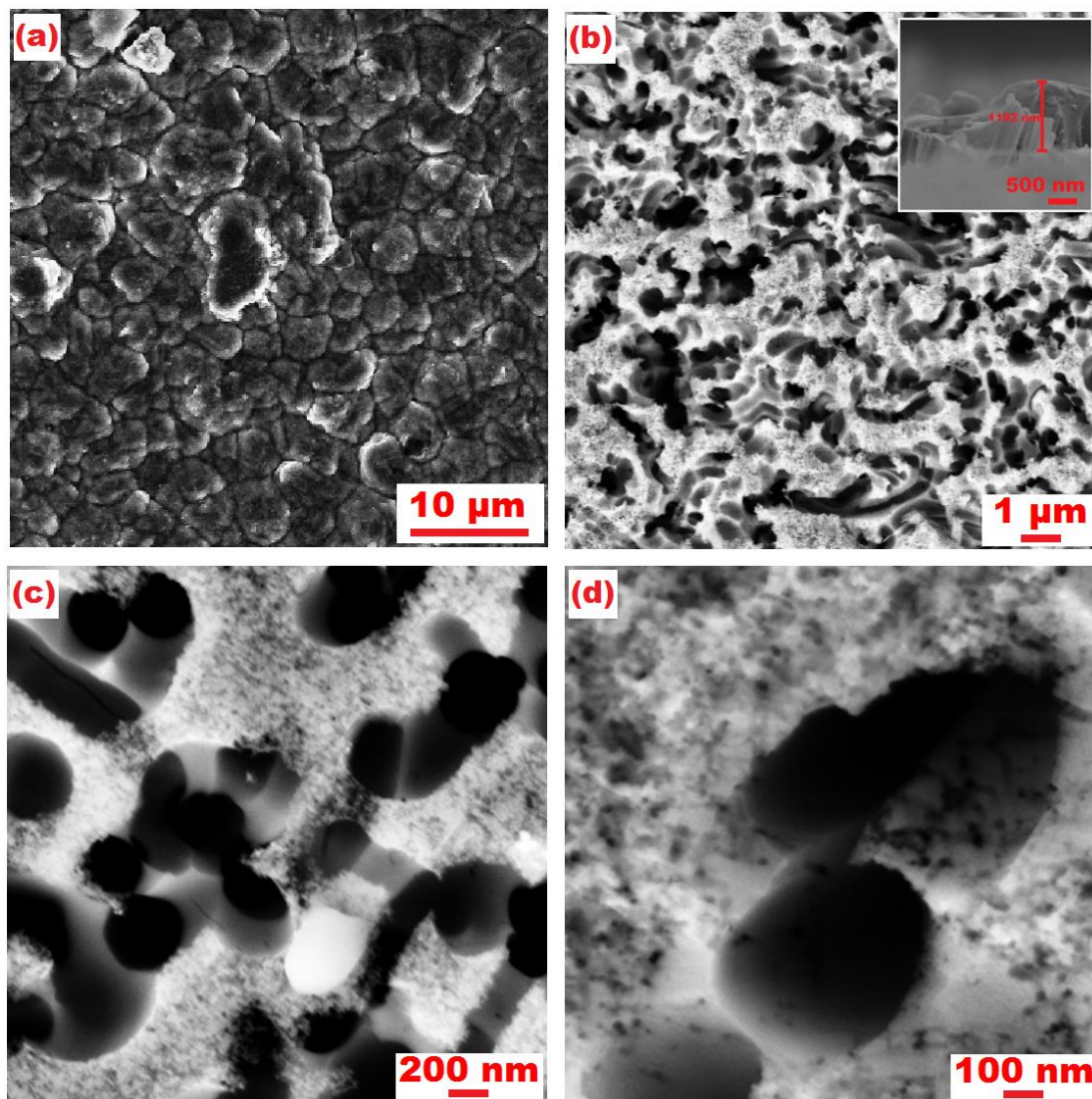

Figure 2. a SEM images of the pristine Si film; **2b-2d** SEM images of the porous Si film at different magnifications.

Fig. 2a shows the surface SEM image of the pristine Si film on the copper foil. The film has a highly rough surface with bulk silicon particles observed. Fig. 2b-2d shows an obvious morphology change of the Si film after metal-assisted chemical etching. It can be seen that a highly porous structure with interconnected worm-like mesopores. Fig. 2c and d display the high-magnification SEM images of the porous Si film. Obviously, a 3D reticular-like porous structure with a pore size in the range of 200-600 nm can be observed on its surface. Furthermore, one can see that the small

micropores were located in the walls of the large mesopores without harming the structural integrity of the mesoporous framework, which is in good agreement with the above BET studies.
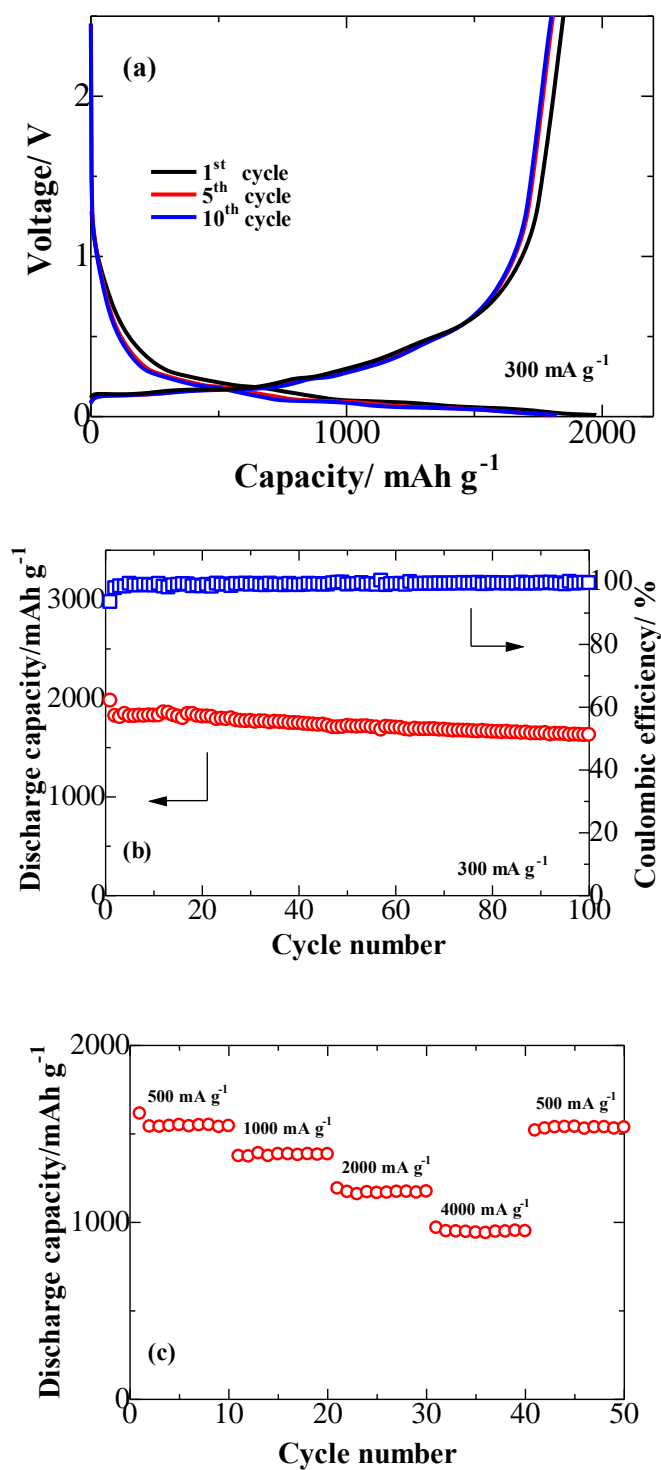

Figure 3. a The initial discharge/charge curves of the porous Si film electrode at current density of 300 mA g^{-1}; **3b** The cycling performance of the porous Si film electrode at current density of 300 mA g^{-1}; **3c** Rate performance of the porous Si film electrode at various current densities.

As results, this porous Si film with hierarchical nano/microstructures can utilize the advantages of both nanometer-sized building blocks and micro- or submicrometer-sized assemblies, which is supposed to not only favor the reaction kinetics for facilitating Li^+ ion and charge transport, but also leave enough spaces to buffer volume expansion, leading to a superior electrochemical performance [18].

Fig. 3a demonstrates the galvanostatic charge/discharge profiles of the porous Si film between 0.01 and 2.5 V under a current density of 300 mA g^{-1}. The first discharge shows flat plateaus below 0.3 V, corresponding to the formation of typical solid electrolyte interphase (SEI) and the alloying reaction of Si electrode with Li to form Li_xSi phase. After the initial cycle, a new cathodic peak around 0.25 V appeared, indicating the phase transformation of crystalline Si into amorphous Si.

Meanwhile, two anodic peaks at around 0.26 and 0.49 V can be observed during the delithiation process, related to the phase transformation from Li_xSi phase to amorphous Si. The porous Si electrode exhibits superior cycling properties as shown in Fig. 3b. The Si electrode delivers a high discharge capacity of 1822 mAh g^{-1} in the 2nd cycle at a current density of 300 mA g^{-1}. After 100 cycles, the capacity is still above 1629 mAh g^{-1}, indicating good structure stability of porous Si film.

Fig. 3c shows rate capability of the porous Si electrode with the current density ranging from 500 mA g^{-1} to 4000 mA g^{-1}. The Si electrode delivers with the discharge capacity around 1550, 1386, 1168 and 949 mAh g^{-1} at the current densities of 500, 1000, 2000 and 4000 mA g^{-1}, respectively. Furthermore, the composite regains closely full of its reversible capacity 1537 mAh g^{-1} when the current density is modulated back to 500 mA g^{-1}. Owing its porous structure, the obtained Si electrode possesses a high surface area and short Li^+ diffusion pathway, which guarantees desirable electron contact and favors its rate capability.
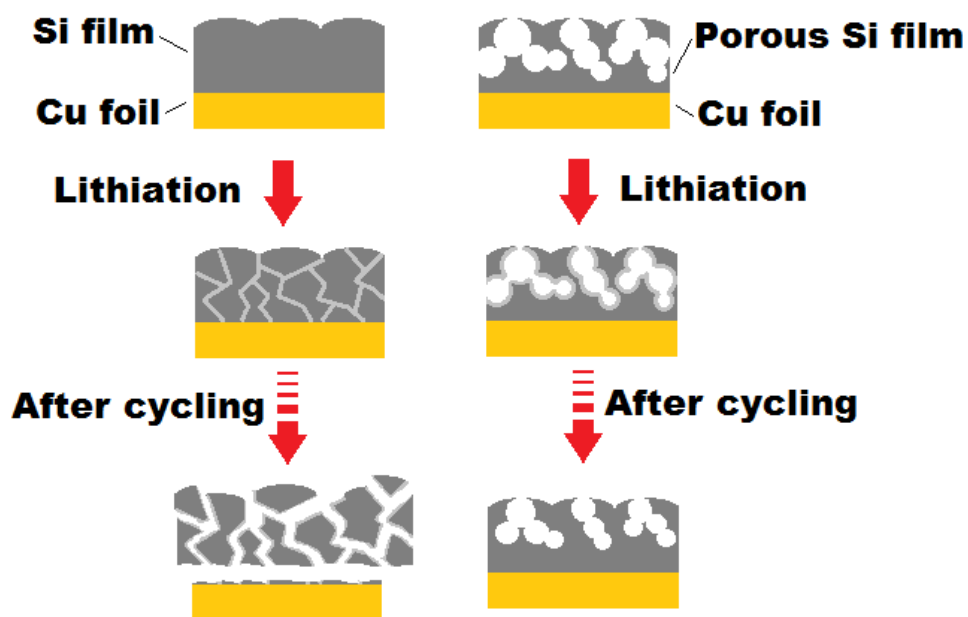

Figure 4. Schematic representations (cross-section view) of structural evolution of the pristine Si film (left) and porous Si film (right).

Fig. 4 illustrates the structural evolution of pristine and porous silicon films upon discharge/charge cycling. During the lithiation process of the pristine Si film, some cracks begin to form due to the alloying reaction of Si electrode with Li. After cycling, the initial pristine Si film is no longer preserved and tends to fall off on the Cu foil. Therefore, large portion of the pristine Si becomes irreversible, which reduces the electrochemical performance. However, porous silicon does not suffer from this problem. The porous Si film consists of many holes with different sizes, which can provide strong mechanical support during the lithiation and delithiation process, resulting in significant improvement in cycling stability.

Comparing with the results obtained on the silicon electrode, it can be concluded that the porous Si film electrode prepared in our work displays excellent electrochemical performance, as shown in Table 1. These results illustrate that the reversible capacity and capacity retention at 100th cycles of the porous Si film are higher than most of other silicon electrodes. The special porous structure could extremely enhance the electrochemical performance of silicon electrode.

Table 1 Comparison of performance of porous Si film electrode for LIBs.

Materials	nth cycle reversible capacity (mAh g^{-1})	Capacity retention for n cycles (%)	Current density	Applied potential range (V)	Ref.
Carbon-coated Si	910 (100th)	77.5	210 mA g^{-1}	0.001-2	[19]
Nanoporous silicon flakes	1453 (100th)	70.1	1 C	-	[20]
3D porous Si@C	1058 (800th)	91.0	1 C	0.01-1	[21]
Si/C nano-branches	860 (50th)	84.3	50 mA g^{-1}	0.005-2	[22]
Ag-deposited 3D porous Si	755 (50th)	39.6	100 mA g^{-1}	0.02-1.5	[23]
Gold-coated porous silicon films	~1300 (163th)	75.9	200 μA cm^{-2} (~1/10 C)	0.1-2	[24]
Porous Si film	1629 (100th)	89.4	300 mA g^{-1}	0.01-2.5	This work

4. CONCLUSIONS

In summary, the porous silicon film anode was prepared by the combination of the magnetron sputtering deposition and metal-assisted chemical etching. The unique morphology and structure of porous Si film provides proper accommodation for the volumetric expansion and shrinkage of silicon film during the lithiation/delithiation processes. Therefore, the Si film electrode exhibits large lithium storage capacity, high coulombic efficiency, and superior cycling properties, implying that they have promising application for anode materials in rechargeable lithium-ion batteries.

References

1. Y. Zhang, Z. Bakenov, Y. Zhao, A. Konarov, T.N.L. Doan, K.E.K. Sun, A. Yermukhambetova and P. Chen, *Powder Technol.*, 235 (2013) 248.
2. J.M. Tarascon and M. Armand, *Nature*, 414 (2001) 359.
3. F. Yin, X. Liu, Y. Zhang, Y. Zhao, A. Menbayeva, Z. Bakenov and X. Wang, *Solid State Sci.*, 66 (2017) 44.
4. M. Tokur, H. Algul, S. Ozcan, T. Cetinkaya, M. Uysal and H. Akbulut, *Electrochim. Acta*, 216 (2016) 312.
5. M. Tokur, H. Algul, M. Uysal, T. Cetinkaya, A. Alp and H. Akbulut, *Surf. Coat. Tech.*, 288 (2016) 62.
6. Y. Zhang, Y. Wei, H. Li, Y. Zhao, F. Yin and X. Wang, *Mater. Lett.*, 184 (2016) 235.
7. Y. Zhang, Y. Li, H. Li, Y. Zhao, F. Yin and Z. Bakenov, *Electrochim. Acta*, 216 (2016) 475.
8. H. Li, Y. Wei, Y. Zhang, C. Zhang, G. Wang, Y. Zhao, F. Yin and Z. Bakenov, *Ceram. Int.*, 42 (2016) 12371.
9. M. Li, J. Li, K. Li, Y. Zhao, Y. Zhang, D. Gosselink and P. Chen, *J. Power Sources*, 240 (2013) 659.
10. C. Chan, H. Peng, G. Liu, K. Mcilwrath, X. Zhang, R. A. Huggins and Y. Cui, *Nat. Nanotechnol.*, 3 (2008) 31.
11. L. Huang, X. Wang, F. Yin, C. Zhang, J. Gao, J. Liu, G. Zhou, Y. Zhang and Z. Bakenov, *J. Nanopart. Res.*, 19 (2017) 42.
12. Y. Zhao, H. Li, Y. Zhang, H. Xie and F. Yin, *Int. J. Electrochem. Sci.*, 11 (2016) 3179.
13. H. Zhang, X. Li, H. Guo, Z. Wang and Y. Zhou, *Powder Technol.*, 299 (2016) 178.
14. W. Zhang, X. Chen, T. Yong, N. Xu, R. Guan and L. Yue, *J. Alloys Compd.*, 688 (2016) 216.
15. W. Wang, Y. Wang, L. Gu, R. Lu, H. Qian and X. Peng, *J. Power Sources*, 293 (2015) 492.
16. S.H. Baek, J.S. Park, Y.M. Jeong and J.H. Kim, *J. Alloys Compd.*, 660 (2016) 387.
17. H. Tang, Y. Zhang, Q. Xiong, J. Cheng, Q. Zhang, X. Wang, C. Gu and J. Tu, *Electrochim. Acta*, 156 (2015) 86.
18. Y. Zhang, Y. Zhao, T. N. L. Doan, A. Konarov, D. Gosselink, H. Soboleski and P. Chen, *Solid State Ionics*, 238 (2013) 30.
19. S. Park, J. Kim, M. Dar, H. Shim and D. Kim, *J. Alloys Compd.*, 698 (2017) 525.
20. Y. Kim, J. Lee and H. Kim, *Physica E*, 85 (2017) 223.
21. H, Wu, N. Du, X. Shi and D. Yang, *J. Power Sources*, 331 (2016) 76.
22. W. Ren, Y. Wang, Q. Tan, Z. Zhong and F .Su, *J. Power Sources*, 332 (2016) 88.
23. Q. Wang, L. Han, X. Zhang, J. Li, X. Zhou and Z. Lei, *Mater. Lett.*, 185 (2016) 558.
24. M. Thakur, M. Isaacson, S. Sinsabaugh, M. Wong and S. Biswal, *J. Power Sources*, 205 (2012) 426.